Lithuanian Journal of Physics
Vol. **63**, No. 3, pp. 155–163 (2023)
ISSN 1648-8504 eISSN 2424-3647
DOI: https://doi.org/10.3952/physics.2023.63.3.6

PYROLYZED PHOTORESIST THIN FILM: EFFECT OF ELECTRON BEAM PATTERNING ON DC AND THz CONDUCTIVITY

J. Jorudas [a, b], H. Rehman [a], G. Fedorov [a], M. Cojocari [a], P. Karvinen [a], A. Urbanowicz [b], I. Kašalynas [b], L.Yu. Matzui [c], Y. Svirko [a], and P. Kuzhir[a]

[a] *Department of Physics and Mathematics, Center of Photonics Sciences, University of Eastern Finland, Yliopistokatu 7, 80101 Joensuu, Finland*
[b] *Department of Optoelectronics, Center for Physical Sciences and Technology (FTMC), Saulėtekio 3, 10257 Vilnius, Lithuania*
[c] *Faculty of Physics, Taras Shevchenko National University of Kyiv, 64/13 Volodymyrska Street, 01601 Kyiv, Ukraine*
Email: justinas.jorudas@ftmc.lt

Received 28 September 2023; accepted 2 October 2023

Pyrolyzed photoresist films (PPFs), which are formed via vacuum annealing of a photoresist without a catalyst, can be employed for fabrication of graphitic nanostructures by using conventional lithographic techniques. Such approach allows for reduction of technological steps required for fabrication of conductive micro- and nanoelectrodes for different applications. However, the operation frequency range of PPF electrodes is still unknown. Here, we report the results of the comparative study of PPF structures fabricated by electron beam lithography prior and after the annealing process with preference to the first approach. By performing the comparative measurements of PPF transport properties we found that both pre-and post-processed PPFs possess the same conductivities at dc-current and in the frequency range from 0.2 to 1.5 THz. Moreover, we achieved the sheet resistance of 150 nm thick PPFs as low as 570 Ω/sq, which is comparable to that of commercially available chemical vapour deposited (CVD) graphene. These findings open a path for a simple, reproducible and scalable fabrication of graphitic nanocircuits, nanoresonators and passive components suitable for applications in frequencies up to few terahertz.

Keywords: pyrolyzed carbon, pyrolyzed photoresist, terahertz, graphitic film, transport properties

1. Introduction

Graphene has received a wide attention due to its remarkable electrical, mechanical and optical properties that open a way for numerous applications [1–4]. However, the integration of a single atom thick graphene sheet into the silicon platform is still a challenge that fuels a search for the graphene alternative in electromagnetics, i.e. for robust graphitic films possessing sheet conductivity comparable with that of graphene in a wide spectrum range [5]. It has been demonstrated in particular that micro- and nano-structuring of such graphitic films deposited onto semiconductor substrates can be used to control microwave and THz radiation [6, 7].

Pyrolyzed polymer films (PPF) made by annealing photoresists in an oxygen free environment [8] comprise highly disordered graphite flakes in an amorphous carbon matrix having a thickness up to ten times smaller than that of a photoresist used for pyrolysis [9]. PPFs have conductivity of about 10 kS/m, which is several orders of magnitude smaller than that of metals (gold, copper and aluminum) normally used in microelectronics and related areas.

The relatively low electrical conductivity of PPF [10] does not rule out practical applications of these carbon films. Indeed, the chemical stability and robustness of PPFs are beneficial for biomedical [11–13], electrochemical [14–16] and microelectromechanical applications [17–20]. Moreover, PPF can be synthesized on silicon, silicon oxide and other substrates conventionally used in modern electronics and optoelectronics [17, 18]. The micro- and nanopatterned PPF-based structures can be created at a specified location on the substrate by using a pre-patterned photoresist significantly

simplifying incorporating carbon electrodes into the semiconductor environment [21–23]. For example, the fabrication of metallic nanoelectrodes implies spin-coating of the resist either before or after the metal deposition, e-beam exposure and resist developing followed by metal etching or lift-off. Annealing of the resist, i.e. the fabrication of PPF, allows for obtaining the conductive nanostructure in a single step after the e-beam exposure.

Despite the listed advantages, it is not yet clear whether the PPF-based electrodes can be used for high frequency applications. In electrodynamics, the criterion of a 'metallic' behaviour in terms of the material dynamic conductivity $\sigma(\omega)$ can be formulated as $\sigma(\omega) \gg \varepsilon_0\omega$, where $\varepsilon_0 = 8.85{\cdot}10^{-12}$ F/m and ω is the characteristic frequency. The dynamic conductivity of a material in most cases decreases as the frequency is increased. Therefore, it is important to characterize the dynamic conductivity of PPF to estimate the frequency range in which the nano-micro electrodes fabricated using this material can be used.

In this communication, we report on the characterization of transport properties of the graphitic films made via pyrolysis of the negative e-beam resist AZ nLOF 2070 (*MicroChemicals GmbH*). To this end, we fabricated two types of PPF based structures. Structures of the first type are defined by electron beam lithography (EBL) followed by development and annealing. Structures of the second type were made of the as-synthesized uniform PPF by plasma O_2 reactive ion etching through the photomask made using EBL technology. The morphology, structure and intrinsic DC conductivity of PPF were found to be the same in both structures. Transmission spectra of the films obtained via time-domain spectroscopy show that the dynamic conductivity of the fabricated structures matches its DC values up to at least 1.5 THz indicating the superior promise of this material for high frequency applications. Moreover, we compare the transport properties of PPF with commercially available graphene-based field-effect devices (*AMO GmbH*) and discuss possible applications.

2. Methods

We fabricated two PPF based structures and compared their transport properties in a wide frequency range. The first structure was defined by EBL followed by development and annealing. We further refer to it as the exposed structure (PPFe). The second structure was made of the as-synthesized uniform PPF by plasma O_2 reactive ion etching through the photomask made of the positive photoresist, polymethyl methacrylate (PMMA), with the help of EBL technology. We further refer to it as the unexposed structure (PPFu). The sketch of PPFe and PPFu fabrication routine is presented in Fig. 1.

The pyrolyzed photoresist films were fabricated on 20 × 20 mm substrates of 525 μm thick p-doped Si wafers coated with 3 μm of SiO_2 and 300 nm of Si_3N_4 (*Silicon Materials*). Prior to spin-coating of the resist, the substrates were cleaned in acetone, isopropanol and deionized (DI) water in an ultrasonic bath, blow-dried with N_2 and heated to 120°C on a hotplate to remove any moisture. We used the photoresist AZ nLOF 2070 (*MicroChemicals GmbH*) diluted with a solvent AZ EBR (*MicroChemicals GmbH*) which was spin-coated on wafers at different speeds to achieve the desired thickness of the photoresist.

The pyrolysis was performed in a vacuum tube furnace (*Carbolite*) under vacuum of 0.1 mBar at different temperatures from 800 to 1100°C for 60 min.

The thickness of photoresist before (D) and after (d) pyrolysis was measured by a profilometer (*Veeco* Dektak 150) at 5 locations to verify the film thickness uniformity. To confirm the conversion of the photoresist into a graphitic film, Raman spectra were measured (*Renishaw* in Via) using a 2400 lines/mm grating and a ×50 objective at the excitation wavelength 514 nm. The Raman mapping of PPF was performed in the 40 × 40 μm^2 area with a pixel size of 2 × 2 μm^2 using a ×20 objective. The experimental spectra were fitted as two Lorentz peaks and a linear background to extract the D and G peak parameters for the whole image. The patterned pyrolyzed films were investigated with an SEM (*Zeiss* LEO 1550) to define the lateral dimensions and to check the integrity of the films. The DC conductivity of PPFs was determined by the Van der Pauw (VdP) method on patterned 6 × 6 mm^2 square test structures performing reciprocal and reversed polarity measurements with a probe station (*Signatone*) and a multimeter (*GW Iinstek*). Finally, both PPFe and PPFu samples were

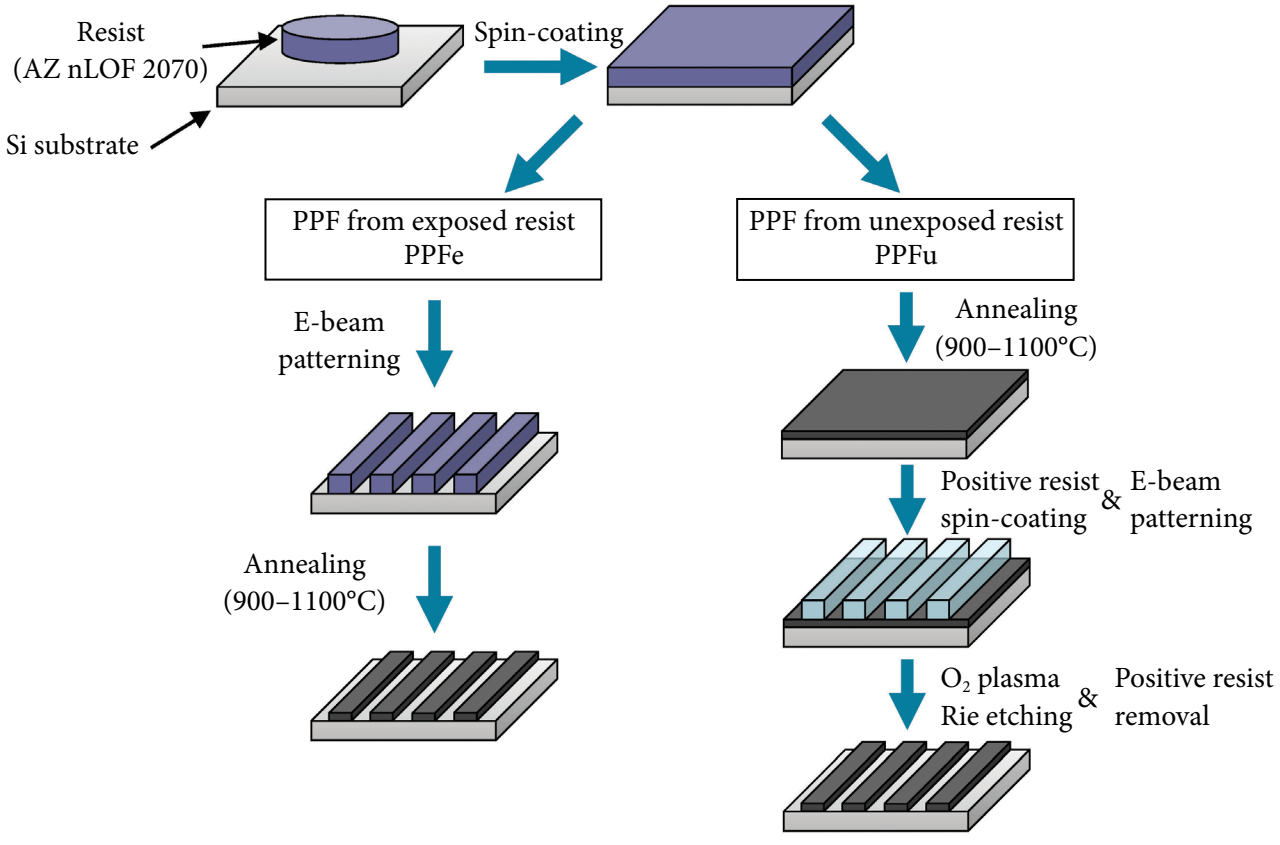

Fig. 1. Illustration of the two fabrication routes for making the two types of PPF gratings: labelled as exposed (PPFe) and unexposed (PPFu) samples.

probed by terahertz time-domain spectroscopy (TDS) (*TeTechS*) in the transmission geometry with an aperture of 4 mm, to investigate the dynamic conductivity of PPF in the THz range.

3. Results

3.1. Geometry and morphology of the films

The profiles of a 50 μm wide stripe (marked by a red line in Fig. 2) of the AZ nLOF 2070 resist before and after the pyrolysis at 900°C are shown in Fig. 2. Starting with the thickness of 833 nm, the thickness of the pyrolyzed film reduces down to 162 nm, i.e. the shrinkage ratio is $S = \frac{D}{d} = 5.1$. Using the data of two other samples processed with the same starting resist thickness and pyrolyzed under the same conditions, the average shrinkage ratio was estimated to be 5.3. It is consistent with the shrinkage obtained previously for the same resist [9, 21, 24, 25]. Other PPF samples annealed at higher temperatures show a higher shrinkage, for example, at 1100°C we measured S = 8.3. However, we did not observe a significant change in the lateral size of both sub-mm and sub-μm resist structures after the pyrolysis.

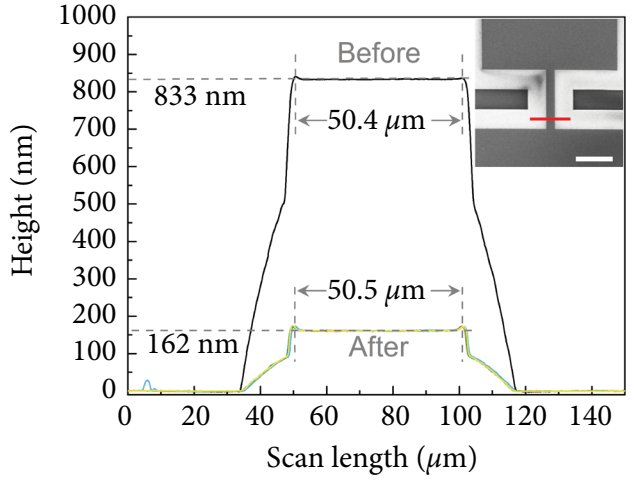

Fig. 2. Profiles of a 50-micron wide resist feature before and after pyrolysis. Inset: SEM image of the PPF Hall bar with a red line marking the areas for profilometer measurement.

The measured Raman spectra after the pyrolysis are dominated by the two broad bands at 1360 and 1600 cm^{-1} for both PPFe and PPFu. The G-peak at 1600 cm^{-1} is the signature of sp^2 carbon, while the D-peak at 1360 cm^{-1} is due to crystallographic defects [26]. The ratio of intensities for these two peaks $I(G)/I(D)$ = 1.1 is the same for PPFe and PPFu samples. The large width of the G-peak as well as the high intensity of the D-peak indicate that in both samples PPF is composed of small monocrystalline graphene flakes. Following Ref. [27] and taking into account $I(D)/I(G) \sim 1$ at an excitation wavelength of 514 nm, we estimate the in-plane crystallite sizes to be $L_a \sim 4$ to 5 nm.

The homogeneity of the fabricated films was checked by Raman mapping. The normalized G peak intensity distribution is shown in Fig. 3(b). The observed fluctuations of the signal do not exceed the intrinsic device noise.

3.2. Transport properties

By using the Van der Pauw method, the sheet resistance of the films was found to be inversely proportional to the film thickness (see Table 1). This indicates that the carrier scattering at the film surface does not affect the transport characteristics of the film, i.e. the carrier mean free path (MFP), which may be estimated as a crystallite size, is shorter than the film thickness. Importantly, the resistivity of PPFs depends on the annealing temperature [24], but it is the same for the pre-exposed and post-exposed films annealed at the same temperature. The latter circumstances are crucial for using of PPF in practical devices.

To estimate the dynamics of the film conductivity, we measured the transmission spectra of bare and PPF-covered wafers using THz TDS in the range 0.2–1.5 THz. The measured time-traces

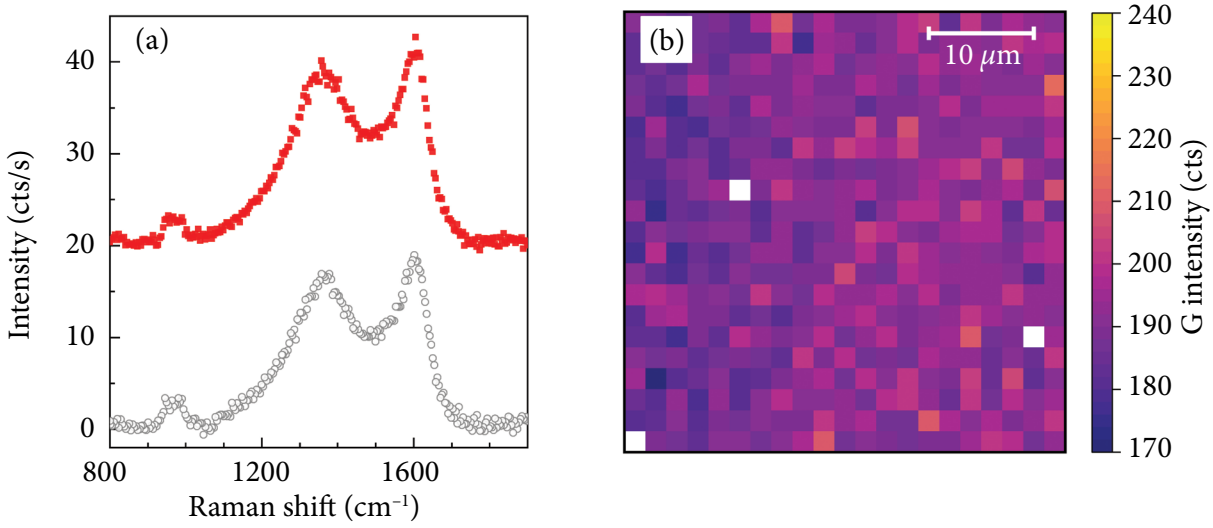

Fig. 3. (a) Raman spectra of PPFu (gray circles) and PPFe (red squares) samples, note that one spectrum is shifted vertically for clarity. (b) 2D plot of the G-peak intensity as a function of coordinates in the lateral plane of the PPFe film.

Table 1. Summary of the results for the PPFe and PPFu samples.

Sample	Annealing temperature, °C	Thickness after pyrolysis d, nm	Shrinkage D/d	Sheet resistance, Ω/sq	Resistivity, mΩ cm
PPF1u	900	42	6.2	1800	7.6
PPF1e			6.2	1550	6.6
PPF2u		150	5.3	570	8.5
PPF2e		157	5.3	470	7.4
PPF3u	1000	35	7.7	3940	13.8
PPF3e			7.7	2620	9.1
PPF4e	1100	32	8.3	5140	16.1

and the calculated spectra for the Si substrate used are shown in Fig. 4(a, b), respectively. The experimental spectra can be simulated by the standard transfer matrix method using the following relations:

$$\varepsilon(\omega) = \varepsilon_{\infty} + \frac{\sigma(\omega)}{\mathrm{i}\omega\varepsilon_0}, \tag{1}$$

$$\sigma(\omega) = \frac{\sigma_{\mathrm{DC}}}{1 - \mathrm{i}\omega\tau}, \tag{2}$$

where τ is the carrier momentum relaxation time, ω is the angular radiation frequency, $\varepsilon(\omega)$ and $\sigma(\omega)$ are the dielectric permittivity and conductivity at the frequency ω, respectively, ε_0 is the vacuum permittivity, ε_{∞} is the silicon high frequency dielectric constant, and σ_{DC} is the DC conductivity of the material.

First, we obtain the scattering time τ of Si by fitting the transmission spectrum of the bare Si substrate with $\sigma_{\mathrm{DC}} = 5$ S/m as measured by the standard 4-probe Van der Pauw method, and $\varepsilon_{\infty} = 11.6$. The best fit was found at $\tau = 0.15$ ps, which is a typical value for the underdoped silicon at room temperature [28].

The transmittance of PPFu and PPFe samples is lower than that of the bare silicon substrate. The relevant transmittance spectra are shown in Fig. 4(c). The fit of PPF-covered wafer transmission spectra gives a very good match between the measured and simulated transmission spectra with the scattering time less than 10 fs, i.e. when $\omega\tau \gg 1$ and $\sigma(\omega) = \sigma_{\mathrm{DC}}$. That is, in the THz range, the dielectric constant is described by Eq. (1) with the frequency independent conductivity matching the DC conductivity. The fact that the PPF conductivity is frequency independent and coincides with the DC one can be used for designing circuits with PPF nano- or microelectrodes in the frequency range from 0 and up to 1.5 THz.

Based on the Fermi velocity for the sp^2 carbon material having an order of 10^6 m/s and a PPF crystallite size of 5 nm, we estimate the PPF scattering time as 5 fs, which is consistent with the $\tau < 10$ fs used in the transmission spectra analysis.

3.3. Discussion

It is instructive to compare the transport characteristics of PPF to those of the chemical vapour deposition (CVD) grown graphene. While the resistivity of the PPF samples is relatively large, the sheet resistance at the thickness below 200 nm is comparable to that of the CVD graphene. Thus, our experimental findings open a way to employ EBL to fabricate nanostructured graphitic electrodes in very few technological steps, offering a viable alternative to nanostructuring CVD graphene via plasma etching through an EBL fabricated mask in many applications.

Since film DC and THz conductivities are practically the same, the PPF electrodes can be used at

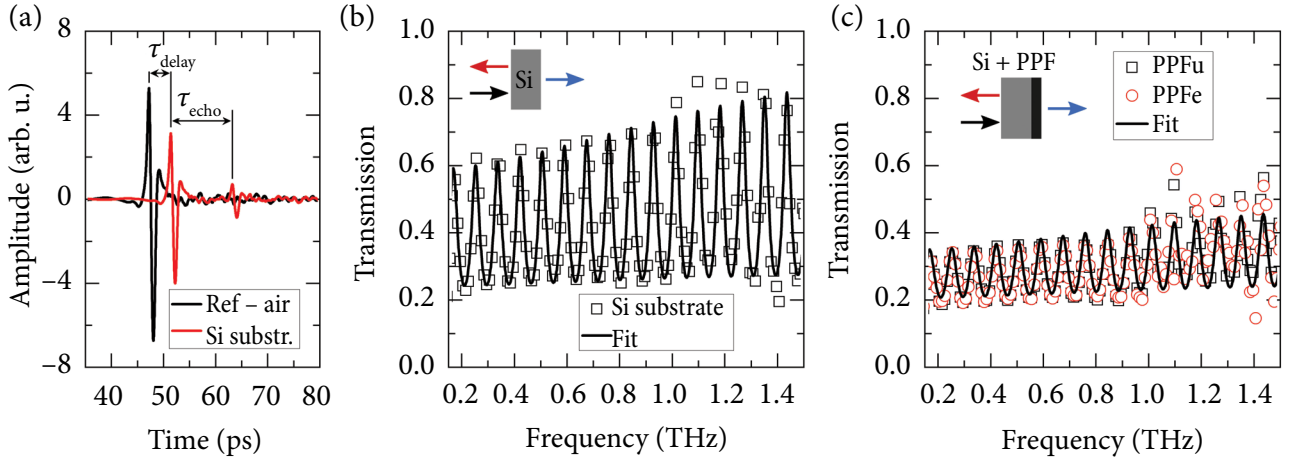

Fig. 4. THz TDS results of PPFe and PPFu samples. (a) Time traces measured after transmission through the aperture (reference) and through the Si substrate. (b) Transmission spectrum of the used wafer (squares) along with the one (solid line) simulated using the model and parameters described in the text. (c) Transmission spectra of the used wafer covered with the pre-exposed (red circles) and post-exposed (black squares) PPF along with the one (solid line) simulated using the model and parameters described in the text.

frequencies lower than $(RC)^{-1}$, where R and C are the electrode resistance and capacitance, respectively. For a pair of parallel nanoelectrodes having a cross section of ~10^{-2} μm^2 with a specific capacitance $C_S \cong 10^{-17}$ F/μm and a specific resistance $R_S \leq 10$ kΩ/μm, the condition $(RC)^{-1} = (R_S C_S L^2)^{-1} \geq \omega$ will be met for a few microns (L) long electrodes in the THz range and for submillimetre electrodes in the GHz range.

Although we did not measure the adhesion of the films using specialized equipment, we observed that the adhesion of both films was good enough to withstand all the technological steps involved and probe station measurements.

To showcase some possible applications for PPFs in the THz range, we fabricated a couple of different structures of PPF, such as nano-grating and split-ring resonators (SRRs). The measured SEM images are shown in Fig. 5(a, b). Figure 5(a) of the periodic nano-grating also demonstrates dark areas between thin grey lines (PPF stripes), two of which on top were marked by a pair of green dotted lines for clarity. These dark regions appear as the result of the charge depletion of the dielectric into the conductive PPF stripes [29]. The Raman mapping of SRRs was performed. The results of the G-peak intensity map are shown in Fig. 5(c) next to its SEM image. We demonstrate that even in the fine features of PPF the structural uniformity is maintained and is similar to the Raman data of the plain PPF (see Fig. 3(b)).

Additionally, biocompatible [13] and much easier to handle PPFs can replace carbon nanotube nanostructures in multielectrode systems used to study and stimulate neuronal electric activity [30]. Further improvement of the performance of PPF based nano- and microstructures can be achieved by catalyst-assisted pyrolysis as described in our recent work [16].

4. Conclusions

To summarize, we find that the transport properties and morphology of the graphitic films made by annealing of the AZ nLOF 2070 resist used in the EBL do not depend on whether the resist was exposed to the electron beam before annealing or not. Investigating the high frequency characteristics of charge carriers in both PPFe and PPFu samples we found that the resistivity values of these films were in a range of 7.4–16.1 mΩ cm and were frequency independent up to at least 1.5 THz. These findings show that based on target application one may use either pre-exposing of the resist or patterning of the already pyrolyzed resist film with no effect on its electrical conductivity up to THz frequencies. Therefore, PPF based conductive structures are applicable in a broad THz range with the benefit of the simple technological process discussed in this paper.

Acknowledgements

The study was accomplished with the financial support of the Academy of Finland (Flagship Programme PREIN, Decision 320166, and Mobility

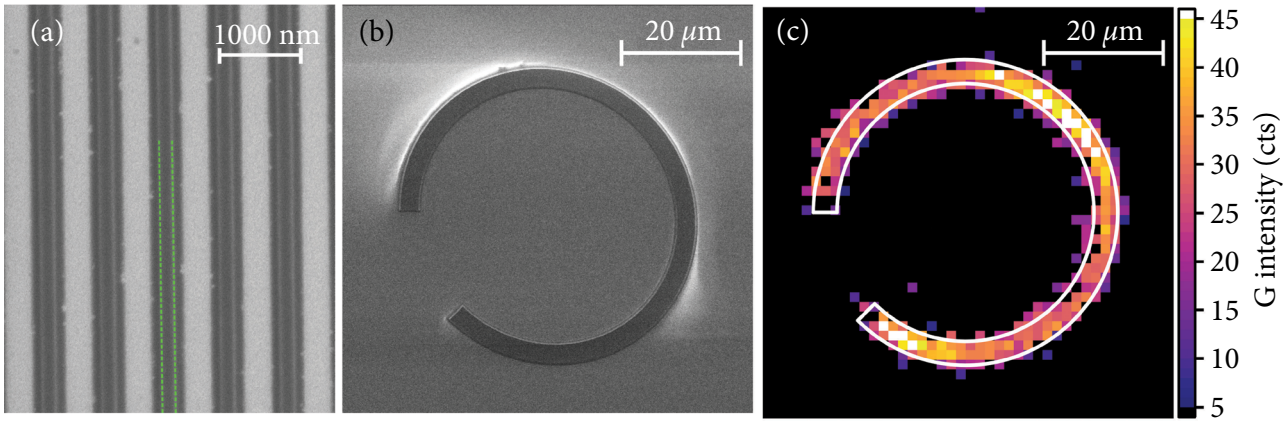

Fig. 5. Demonstration of possible applications of the PFFs: (a) SEM picture of the nano-grating composed of periodic nano-electrodes; (b) SEM picture and (c) the Raman image of the G peak intensity mapping of the unit-cell of split-ring resonator (SRR) designed for waves filtering and beaming in the THz range.

to Finland Decision 334270), Subproject h-cube of EU ATTRACT Phase 2 Research Infrastructure H2020 Project No. 101004462 and Horizon 2020 RISE DiSeTCom (Project No. 823728). The Vilnius Group acknowledges the Research Council of Lithuania for financial support through the 'T-HP' Project under Grant DOTSUT-184 funded by the European Regional Development Fund according to the supported activity 'Research Projects Implemented by World-Class Researcher Groups' under Contract 01.2.2-LMT-K-718-03-0096.

References

[1] R.R. Nair, P. Blake, A.N. Grigorenko, K.S. Novoselov, T.J. Booth, T. Stauber, N.M.R. Peres, and A.K. Geim, Fine structure constant defines visual transparency of graphene, Science **320**(5881), 1308–1308 (2008), https://doi.org/10.1126/science.1156965

[2] C. Liao, Y. Li, and S. Tjong, Graphene nanomaterials: synthesis, biocompatibility, and cytotoxicity, Int. J. Mol. Sci. **19**(11), 3564 (2018), https://doi.org/10.3390/ijms19113564

[3] Y. Xia, W. Gao, and C. Gao, A review on graphene-based electromagnetic functional materials: electromagnetic wave shielding and absorption, Adv. Funct. Mater. **32**(42), 2204591 (2022), https://doi.org/10.1002/adfm.202204591

[4] C.-H. Lin, Y.-S. Chen, J.T. Lin, H.C. Wu, H.T. Kuo, C.F. Lin, P. Chen, and P.C. Wu, Automatic inverse design of high-performance beam-steering metasurfaces via genetic-type tree optimization, Nano Lett. **21**(12), 4981–4989 (2021), https://doi.org/10.1021/acs.nanolett.1c00720

[5] T. Kaplas and P. Kuzhir, Ultra-thin pyrocarbon films as a versatile coating material, Nanoscale Res. Lett. **12**(1), 121 (2017), https://doi.org/10.1186/s11671-017-1896-0

[6] P.P. Kuzhir, A.G. Paddubskaya, N.I. Volynets, K.G. Batrakov, T. Kaplas, P. Lamberti, R. Kotsilkova, and P. Lambin, Main principles of passive devices based on graphene and carbon films in microwave–THz frequency range, J. Nanophotonics **11**(3), 032504 (2017), https://doi.org/10.1117/1.JNP.11.032504

[7] M. Baah, A. Paddubskaya, A. Novitsky, N. Valynets, M. Kumar, T. Itkonen, M. Pekkarinen, E. Soboleva, E. Lahderanta, M. Kafesaki, Y. Svirko, and P. Kuzhir, All-graphene perfect broadband THz absorber, Carbon **185**, 709–716 (2021), https://doi.org/10.1016/j.carbon.2021.09.067

[8] A.M. Lyons, Photodefinable carbon films: Control of image quality, J. Vac. Sci. Technol. B **3**(1), 447 (1985), https://doi.org/10.1116/1.583284

[9] M. Schreiber, T. Lutz, G.P. Keeley, S. Kumar, M. Boese, S. Krishnamurthy, and G.S. Duesberg, Transparent ultrathin conducting carbon films, Appl. Surf. Sci. **256**(21), 6186–6190 (2010), https://doi.org/10.1016/j.apsusc.2010.03.138

[10] M. Baah, P. Obraztsov, A. Paddubskaya, A. Biciunas, S. Suvanto, Y. Svirko, P. Kuzhir, and T. Kaplas, Electrical, transport, and optical properties of multifunctional graphitic films synthesized on dielectric surfaces by nickel nanolayer-assisted pyrolysis, ACS Appl. Mater. Interfaces **12**(5), 6226–6233 (2020), https://doi.org/10.1021/acsami.9b18906

[11] S.T. Larsen, A. Argyraki, L. Amato, S. Tanzi, S.S. Keller, N. Rozlosnik, and R. Taboryski, Pyrolyzed photoresist electrodes for integration in microfluidic chips for transmitter detection from biological cells, ECS Electrochem. Lett. **2**(5), B5–B7 (2013), https://doi.org/10.1149/2.005305eel

[12] H. Zhou, J. Zhou, A. Gupta, and T. Zou, Photoresist derived carbon for growth and differentiation of neuronal cells, Int. J. Mol. Sci. **8**(8), 884–893 (2007), https://doi.org/10.3390/i8080884

[13] L. Golubewa, H. Rehman, T. Kulahava, R. Karpič, M. Baah, T. Kaplas, A. Shah, S. Malykhin, A. Obraztsov, D. Rutkauskas, et al., Macro-, micro- and nano-roughness of carbon-based interface with the living cells: towards a versatile bio-sensing platform, Sensors **20**(18), 5028 (2020), https://doi.org/10.3390/s20185028

[14] D. Sánchez-Molas, J. Cases-Utrera, P. Godignon, and F. Javier del Campo, Mercury detection at microfabricated pyrolyzed photoresist film (PPF) disk electrodes, Sens. Actuators B Chem. **186**, 293–299 (2013), https://doi.org/10.1016/j.snb.2013.06.017

[15] Y.M. Hassan, C. Caviglia, S. Hemanth, D.M.A. Mackenzie, T.S. Alstrøm, D.H. Petersen, and S.S. Keller, High temperature SU-8 pyrolysis for fabrication of carbon electrodes, J. Anal. Appl. Pyrolysis **125**, 91–99 (2017), https://doi.org/10.1016/j.jaap.2017.04.015

[16] M. Baah, A. Rahman, S. Sibilia, G. Trezza, L. Ferrigno, L. Micheli, A. Maffucci, E. Soboleva, Y. Svirko, and P. Kuzhir, Electrical impedance sensing of organic pollutants with ultrathin graphitic membranes, Nanotechnology **33**(7), 075207 (2022), https://doi.org/10.1088/1361-6528/ac3861

[17] J.J. Heikkinen, J. Košir, V. Jokinen, and S. Franssila, Fabrication and design rules of three dimensional pyrolytic carbon suspended microstructures, J. Micromech. Microeng. **30**(11), 115003 (2020), https://doi.org/10.1088/1361-6439/ab9f5b

[18] O. Pilloni, M. Madou, D. Mendoza, S. Muhl, and L. Oropeza-Ramos, Methodology and fabrication of adherent and crack-free SU-8 photoresist-derived carbon MEMS on fused silica transparent substrates, J. Micromech. Microeng. **29**(2), 027002 (2019), https://doi.org/10.1088/1361-6439/aaf70f

[19] M. Kurek, F. Larsen, P. Larsen, S. Schmid, A. Boisen, and S. Keller, Nanomechanical pyrolytic carbon resonators: novel fabrication method and characterization of mechanical properties, Sensors **16**(7), 1097 (2016), https://doi.org/10.3390/s16071097

[20] L.N. Quang, P.E. Larsen, A. Boisen, and S.S. Keller, Tailoring stress in pyrolytic carbon for fabrication of nanomechanical string resonators, Carbon **133**, 358–368 (2018), https://doi.org/10.1016/j.carbon.2018.03.005

[21] R. Du, S. Ssenyange, M. Aktary, and M.T. McDermott, Fabrication and characterization of graphitic carbon nanostructures with controllable size, shape, and position, Small **5**(10), 1162–1168 (2009), https://doi.org/10.1002/smll.200801357

[22] J.A. Lee, K.-C. Lee, S. Il Park, and S.S. Lee, The fabrication of carbon nanostructures using electron beam resist pyrolysis and nanomachining processes for biosensing applications, Nanotechnology **19**(21), 215302 (2008), https://doi.org/10.1088/0957-4484/19/21/215302

[23] K. Malladi, C. Wang, and M. Madou, Fabrication of suspended carbon microstructures by e-beam writer and pyrolysis, Carbon **44**(13), 2602–2607 (2006), https://doi.org/10.1016/j.carbon.2006.04.039

[24] A. Singh, J. Jayaram, M. Madou, and S. Akbar, Pyrolysis of negative photoresists to fabricate carbon structures for microelectromechanical systems and electrochemical applications, J. Electrochem. Soc. **149**(3), E78 (2002), https://doi.org/10.1149/1.1436085

[25] S. Ranganathan, R. McCreery, S.M. Majji, and M. Madou, Photoresist-derived carbon for microelectromechanical systems and electrochemical applications, J. Electrochem. Soc. **147**(1), 277 (2000), https://doi.org/10.1149/1.1393188

[26] A.C. Ferrari and D.M. Basko, Raman spectroscopy as a versatile tool for studying the properties of graphene, Nat. Nanotechnol. **8**(4), 235–246 (2013), https://doi.org/10.1038/nnano.2013.46

[27] M.J. Matthews, M.A. Pimenta, G. Dresselhaus, M.S. Dresselhaus, and M. Endo, Origin of dispersive effects of the Raman D band in carbon materials, Phys. Rev. B **59**(10), R6585–R6588 (1999), https://doi.org/10.1103/PhysRevB.59.R6585

[28] M. van Exter and D. Grischkowsky, Carrier dynamics of electrons and holes in moderately doped silicon, Phys. Rev. B **41**(17), 12140–12149 (1990), https://doi.org/10.1103/PhysRevB.41.12140

[29] Y. Homma, S. Suzuki, Y. Kobayashi, M. Nagase, and D. Takagi, Mechanism of bright selective imaging of single-walled carbon nanotubes on insulators by scanning electron microscopy, Appl. Phys. Lett. **84**(10), 1750–1752 (2004), https://doi.org/10.1063/1.1667608

[30] L. Bareket-Keren and Y. Hanein, Carbon nanotube-based multi electrode arrays for neuronal interfacing: progress and prospects, Front. Neural Circuits **6** (2013), https://doi.org/10.3389/fncir.2012.00122

PLONIEJI PIROLIZUOTO FOTOREZISTO SLUOKSNIAI: STRUKTŪRIZAVIMO ELEKTRONŲ PLUOŠTU ĮTAKA SLUOKSNIO NUOLATINĖS SROVĖS IR THz ELEKTRINIAM LAIDUMUI

J. Jorudas [a, b], H. Rehman [a], G. Fedorov [a], M. Cojocari [a], P. Karvinen [a], A. Urbanowicz [b], I. Kašalynas [b], L.Yu. Matzui [c], Y. Svirko [a], P. Kuzhir [a]

[a] *Rytų Suomijos universiteto Fotonikos mokslų centro Fizikos ir matematikos skyrius, Joensu, Suomija*

[b] *Fizinių ir technologijos mokslų centro Optoelektronikos skyrius, Vilnius, Lietuva*

[c] *Kyjivo nacionalinio Taraso Ševčenkos universiteto Fizikos fakultetas, Kyjivas, Ukraina*

Santrauka

Pirolizuoto fotorezisto sluoksniai (PPF), sudaromi kaitinant fotorezistą vakuume nenaudojant katalizatoriaus, gali būti panaudoti grafitinių nano darinių gamybai pasitelkiant įprastas litografines technologijas. Toks metodas leidžia supaprastinti technologinį procesą, reikalingą gaminti laidžius mikro- ir nanoelektrodus. Tačiau PPF elektrodų elektrinio laidumo charakteristikos plačiame dažnių ruože vis dar nėra žinomos. Šiame darbe ištirti PPF dariniai pagaminti naudojant elektronų pluošto litografiją arba prieš, arba po fotorezisto pirolizės. Atlikus palyginamuosius PPF laidumo matavimus, nustatyta, kad dariniai, pagaminti iš PPF, paveikto elektronų pluoštu ar prieš, ar po fotorezisto pirolizės, pasižymi vienodu elektriniu laidumu ir nuolatinės srovės (DC) režime, ir THz dažnių ruože iki 1,5 THz. Pavyko pagaminti 150 nm storio PFF bandinius, kurių sluoksnio varža buvo tik 570 Ω/sq, – panašios yra komercinio CVD grafeno laidumo vertės. Šie rezultatai atveria galimybių paprastai, atkartojamai gaminti lengvai keičiamo dydžio grafitinius nanograndynus, nanorezonatorius ir pasyviuosius komponentus, kurie gali būti taikomi nuo DC iki keleto terahercų (THz) dažnių ruože.

Special dedication to prof. Gintaras Valušis

I was really lucky to meet you one day in 2007 in Vilnius, in THz Atelier. We had a lot of fun studying THz features of various nanocarbons. Many good papers were published together, and many projects have been initiated and implemented. Hot discussions, smooth opinions exchanges and lazy coffees form a unique atmosphere around you, stimulating team work. As all your international colleagues, I feel your continuous support and attention. Thanks a lot for 15+ years of our successful collaboration and I do hope we will have more for future scientific endeavours!

Prof. Polina Kuzhir